Inorg. Chem. **2009**, *48*, 2233−2245

New Antimony(III) Bromide Complexes with Thioamides: Synthesis, Characterization, and Cytostatic Properties

Ibrahim I. Ozturk,[†] Sotiris K. Hadjikakou,*[,†] Nick Hadjiliadis,*[,†] Nikolaos Kourkoumelis,[‡] Maciej Kubicki,[§] Anastasios J. Tasiopoulos,[||] Hanadi Scleiman,[⊥] Mirela M. Barsan,[⊥] Ian S. Butler,[⊥] and Jan Balzarini[#]

Section of Inorganic and Analytical Chemistry, Department of Chemistry, University of Ioannina, 45110 Ioannina, Greece, Medical Physics Laboratory, Medical School, University of Ioannina, 45110 Ioannina, Greece, Faculty of Chemistry, Adam Mickiewicz University, Grunwaldzka 6, 60-780 Poznan′, Poland, Department of Chemistry, University of Cyprus, 1678 Nicosia, Cyprus, Department of Chemistry, McGill University, 801 Sherbrooke Str.West, Montreal, Quebec H2A 2K6, Canada, and Katholieke Universiteit Leuven, Rega Institute for Medical Research, Minderbroedersstraat 10, B-3000 Leuven, Belgium

Received October 8, 2008

New antimony(III) bromide complexes with the heterocyclic thioamides, thiourea (TU), 2-mercapto-1-methylimidazole (MMI), 2-mercapto-benzimidazole (MBZIM), 2-mercapto-5-methyl-benzimidazole (MMBZIM), 5-ethoxy-2-mercapto-benzimidazole (EtMBZIM), 2-mercapto-3,4,5,6-tetrahydro-pyrimidine (tHPMT), 2-mercaptopyridine (PYT), 2-mercapto-thiazolidine (MTZD), 3-methyl-2-mercaptobenzothiazole (MMBZT), and 2-mercaptopyrimidine (PMTH) of formulas $[SbBr_3(TU)_2]$ (**1**), $[SbBr_3(MMI)_2]$ (**2**), $\{[SbBr_2(MBZIM)_4]^+ [Br]^- H_2O\}$ (**3**), $\{[SbBr_2(\mu_2\text{-}Br)(MMBZIM)_2]_2\}$ (**4**), $\{[SbBr_2(\mu_2\text{-}Br)(EtMBZIM)_2]_2$ MeOH$\}$ (**5**), $\{[SbBr_3(\mu_2\text{-}S\text{-}tHPMT)(tHPMT)]_n\}$ (**6**), $\{[SbBr_2(\mu_2\text{-}Br)(PYT)_2)_n\}$ (**7**), $\{[SbBr_2(\mu_2\text{-}Br)(MTZD)_2]_n\}$ (**8**), $[SbBr_3(MMBZT)_2]$ (**9**), and $\{[SbBr_5]^{2-}[(PMTH_2^+)_2]\}$ (**10**) have been synthesized and characterized by elemental analysis, conductivity measurements, FTIR spectroscopy, FT-Raman spectroscopy, TG-DTA analysis, and X-ray powder diffraction. The crystal structures of **3**, **4**, **5**, **6**, **7**, **8**, and **10** were also determined by X-ray diffraction. In **3**, four sulfur atoms from thione ligands and two bromide ions form an octahedral (O_h) cationic $[SbS_4Br_2]^+$ species in which the two bromide anions lie at axial positions. A third bromide counteranion neutralizes the whole complex. **4** and **5** are dimers, whereas **6**, **7** and **8** are polymers, built up by monomeric units of square pyramidal (SP) geometry around the metal center, which were formed by two sulfur atoms of thioamide ligands and three bromide ions. Finally, **10** is ionic salt containing 1D polymeric network of $\{[SbBr_5]^{2-}\}_n$ anions and $^-[(PMTH_2^+)2]$ counter cations in the lattice. The complexes showed mostly a moderate cytostatic activity against a variety of tumor cell lines.

1. Introduction

Antimony-based metallotherapeutic drugs have been the major therapeutic compounds for leishmania for years.[1−5] The mechanism of their antileishmanial activity is still poorly understood.[4,5] It has been proposed that the relatively nontoxic Sb(V) acts only as a prodrug and it is reduced into the more toxic trivalent form near or in the action site and therefore the antileishmanial activity is due to the trivalent ion Sb(III).[1a,4−6] This redox behavior of the metal center is found to affect the geometry of the complex core,[7] whereas the geometric transformations, which may take place during this process, may involve the intermolecular interactions that play an important role in the solid-state arrangement, the

* To whom correspondence should be addressed: E-mail: shadjika@uoi.gr. Tel: xx30-26510-98374(S.K.H.), E-mail: nhadjis@uoi.gr. Tel: xx30-26510-98420. Fax: xx30-26510-98786 (N.H.).
† Department of Chemistry, University of Ioannina.
‡ Medical School, University of Ioannina.
§ Faculty of Chemistry, Adam Mickiewicz University.
|| Department of Chemistry, University of Cyprus.
⊥ Department of Chemistry, McGill University.
Katholieke Universiteit Leuven, Rega Institute for Medical Research.

(1) (a) Yan, S.; Lan, L.; Sun, H. *Antimony in Medicine, in Metallotherapeutic drugs and Metal-based diagnostic Agents − The Use of Metals in Medicine*; Gielen, M, Tiekink, E. R. T., Eds.; Willey: England, 2005. (b) *Martidale The Extra Pharmacopoeiam, 28th ed.*; Raynolds, J. E. F., Ed.; The Pharmaceutical Press: London, 1982. (c) Marsden, P. D. *Rev. Soc. Bras. Med. Trop* **1985**, *18*, 187–198. Pentavalent antimonials: old drugs for new diseases. (d) Herwaldt, B. L. *Lancet* **1999**, *354*, 1191–1199.
(2) Tiekink, E. R. T. *Crit. Rev. Oncol./Hematol.* **2002**, *42*, 217–224.
(3) Yan, S.; Li, F.; Ding, K.; Sun, H. *J. Biol. Inorg. Chem.* **2003**, *8*, 689–697.
(4) Guo, Z.; Sadler, P. J. *Adv. Inorg. Chem.* **2000**, *49*, 183–306.
(5) Sun, H.; Yan, S. C.; Cheng, W. S. *Eur. J. Biochem.* **2000**, *267*, 5450–5457.

10.1021/ic8019205 CCC: $40.75
Published on Web 01/26/2009

Scheme 1

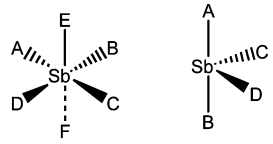

Oh **ø-TBP**

Scheme 2

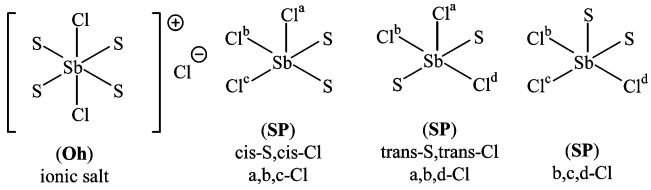

(Oh) ionic salt

(SP) cis-S,cis-Cl a,b,c-Cl

(SP) trans-S,trans-Cl a,b,d-Cl

(SP) b,c,d-Cl

solvation effect, and the $5s^2$ lone pair of electrons located on Sb(III) as well.[7] Sulfur containing ligands, such as thiones/thiols,[8] thioethers,[9] dithiocarbamates,[10] have been used to prepare stable Sb(III) bromide complexes. The reports on structural characterization of antimony(III) bromide complexes with thione/thiol ligands are rare in the literature. These include $[Sb(k^3\text{-}Tm^{Me})(k^1\text{-}Tm^{Me})Br]$ (Tm^{Me} = hydrotris(methimazolyl)borate),[8a] $[SbBr(dmit)(THF)]_n$ (dmit = 2-thioxo-1,3-dithiole-4,5-dithiolato),[8b] {[Ph−CH=CH(Ph)S]SbBr},[8c] $[S(C_6H_4S)_2]SbBr$,[8d] and $[Sb(mtsc)Br_2]$ (Hmtsc= *N*'-[1-(2-pyridyl)ethylidene]morpholine-4-carbothiohydrazide).[8e] Up to now, antimony(III) bromide complexes with thione/thiole were found to adopt octahedral (O_h)[8a] and pseudotrigonal-bipyramidal (Ψ-TBP) structures[8b−d] (Scheme 1).

Recently, we described a series of antimony(III) chloride complexes with thione ligands.[11] These complexes adopt either octahedral (O_h) or square pyramidal (SP) geometries (Scheme 2) and the O_h geometries exhibit selective antiproliferative activity against HeLa cells. Moreover, the SP complex with *trans*-Cl, *trans*-S, is more active against human T-lymphocyte cells (Molt4/C8, CEM) than the other complexes with SP or O_h geometries[11] (Scheme 2). Thus, the study of the structural behavior of the complexes derived from the reaction between antimony(III) halides and thiones is a matter of significant importance.

In this article, we report the structural and spectroscopic characterization of 10 new antimony(III) tribromide complexes with the heterocyclic thioamides (Scheme 3), thiourea (TU), 2-mercapto-1-methylimidazole (MMI), 2-mercaptobenzimidazole (MBZIM), 2-mercapto-5-methyl-benzimidazole (MMBZIM), 5-ethoxy-2-mercapto-benzimidazole (EtMBZIM), 2-mercapto-3,4,5,6-tetrahydro-pyrimidine (tHPMT), 2-mercaptopyridine (PYT), 2-mercapto-thiazolidine (MTZD), 3-methyl-2-mercaptobenzothiazole (MMBZT), and 2-mercaptopyrimidine (PMTH) of formulas $[SbBr_3(TU)_2]$ (**1**), $[SbBr_3(MMI)_2]$ (**2**), $\{[SbBr_2(MBZIM)_4]^+\ [Br]^-\ H_2O\}$ (**3**), $\{[SbBr_2(\mu_2\text{-}Br)(MMBZIM)_2]_2\}$ (**4**), $\{[SbBr_2(\mu_2\text{-}Br)(EtMBZIM)_2]_2\ MeOH\}$ (**5**), $\{[SbBr_3(\mu_2\text{-S-tHPMT})(tHPMT)]_n\}$ (**6**), $\{[SbBr_2(\mu_2\text{-}Br)(PYT)_2]_n\}$ (**7**), $\{[SbBr_2(\mu_2\text{-}Br)(MTZD)_2]_n\}$ (**8**), $[SbBr_3(MMBZT)_2]$ (**9**), and $\{[SbBr_5]^{2-}[(PMTH_2^+)_2]\}$ (**10**). These new complexes exhibit interesting structural motifs.

Results and Discussion

General Aspects. Antimony(III) complexes **1**−**10** have been synthesized by reacting the appropriate thioamide with antimony(III) bromide ($SbBr_3$) in methanolic/dichloromethane, methanolic/acetonitrile, or dichloromethane solutions, as shown by eqs I−IV.

All of the complexes are formed as air-stable powders. Crystals of **3** suitable for X-ray analysis were grown by slow evaporation of a methanol/dichloromethane (1:1) solution, whereas crystals of **4**, **6**, and **8** were grown from acetonitrile solutions and those of **5**, **7**, and **10** were obtained from methanol/acetonitrile solutions.

$$SbBr_3 + 4MBZIM \xrightarrow{CH_3OH/CH_2Cl_2} \underset{\mathbf{3}}{\{[Sb(MBZIM)_4Br_2]^+Br^-H_2O\}} \quad (I)$$

$$n SbBr_3 + 2n HL \xrightarrow[(b)\ CH_3OH/CH_3CN]{(a)\ CH_2Cl_2,\ re\text{-}cryst.\ CH_3CN} [SbBr_2(\mu_2\text{-}Br)(HL)_2]_n \quad (II)$$

(a) $n = 2$ and HL = MMBZIM (**4**), n = infinite and HL= MTZD (**8**) or MMI (**2**)

(b) $n = 2$ and HL = EtMBZIM (**5**), n = infinite and HL= PYT (**7**) or MMBZT (**9**) or TU (**1**)

$$n SbBr_3 + 2n tHPMT \xrightarrow{CH_2Cl_2,\ re\text{-}cryst.\ CH_3CN} \underset{\mathbf{6}}{[SbBr_3(\mu_2\text{-S-tHPMT})(tHPMT)]_n} \quad (III)$$

$$n SbBr_3 + HPMT \xrightarrow{CH_3OH/CH_3CN} \underset{\mathbf{10}}{\{[SbBr_5]_n^{2-}[(H_2PMT)^+]_2\}} \quad (IV)$$

Thermal Analysis. Scheme 4 summarizes the thermal decomposition of **1**−**10** based on thermal analysis in a flowing nitrogen atmosphere. Three main decomposition pathways were observed for the O_h (A), dimeric (B), and polymeric (C) types of complexes.

The decomposition of the octahedral ionic salt **3** sums up to a total of 80% mass loss and it is connected with three

(6) Shaked-Mishan, P.; Ulrich, N.; Ephros, M.; Zilberstein, D. *J. Biol. Chem.* **2001**, *276*, 3971–3976.
(7) Avarvari, N.; Faulques, E.; Fourmigue, M. *Inorg. Chem.* **2001**, *40*, 2570–2577.
(8) (a) Dodds, C. A.; Reglinski, J.; Spicer, M. D. *Chem.—Eur. J.* **2006**, *12*, 931–939. (b) Abrantes, L. T.; Comerlato, N. M.; Ferreira, G. B.; Alan Howie, R.; Wardell, J. L. *Inorg. Chem. Commun.* **2006**, *9*, 522–525. (c) Buchwald, S. L.; Flsher, R. A.; Davis, W. M. *Organometallics* **1989**, *8*, 2082–2084. (d) Alvarado-Rodriguez, J. G.; Andrade-Lopez, N.; Gonzalez-Montiel, S.; Merino, G.; Vela, A. *Eur. J. Inorg. Chem.* **2003**, *3554*, 356. (e) Kasuga, N. C.; Onodera, K.; Nakano, S.; Hayashi, K.; Nomiya, K. *J. Inorg. Biochem.* **2006**, *100*, 1176–1186.
(9) Barton, A. J.; Hill, N. J.; Levason, W.; Reid, G. *J. Chem. Soc., Dalton Trans.* **2001**, *1621*, 1627.
(10) (a) Zhai, J.; Pan, Q.-X.; Yin, H.-D.; Li, F.; Wang, D.-Q. *Acta Crystallogr.* **2007**, *E63*, m1356–m1357. (b) Sun, Y.; Li, Y.; Cui, X.; Lang, X. *Acta Crystallogr.* **2007**, *E63*, m3132-m3132. (c) Yin, H.-D.; Zhai, J.; Sun, Y.-Y.; Wang, D.-Q. *Polyhedron* **2008**, *27*, 663–670.
(11) Ozturk, I. I.; Hadjikakou, S. K.; Hadjiliadis, N.; Kourkoumelis, N.; Kubicki, M.; Baril, M.; Butler, I. S.; Balzarini, J. *Inorg. Chem.* **2007**, *46*, 8652–8661.

Scheme 3

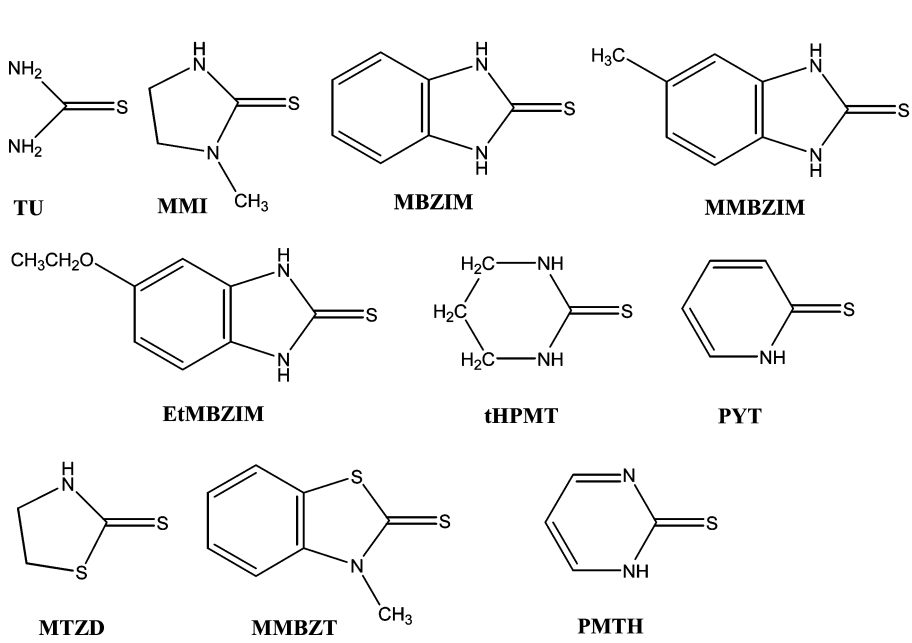

Scheme 4

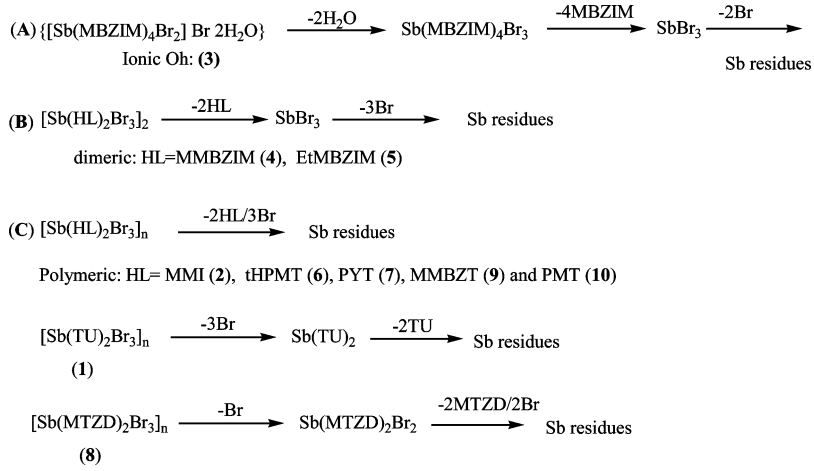

endothermic effects. The first stage of decomposition (100−138 °C, **3**) involves a 4.00% mass loss of two water molecules (calculated mass loss 3.61%). The second stage (138−320 °C) involves a 59% mass loss of four MBZIM ligands (calculated mass loss 60%). Finally, the third decomposition stage (330−460 °C) of 15% mass loss corresponds to two bromine atoms (calculated mass loss 16%).

The corresponding thermal analysis of the dimeric **4** and **5** consists of two main steps, which sum up to total mass losses of 57% (**4**) and 65% (**5**), respectively. The first stage of decomposition (80−342 °C (**4**) and 230−350 °C (**5**)) involves 46% (**4**) and 48% (**5**) and mass losses that correspond to the evolution of two ligands (calculated mass loss of 48 (**4**) and 50% (**5**), respectively). The second stage of decomposition (342−450 °C (**4**) and 350−470 °C (**5**)) involves 11% (**4**) and 13% (**5**) and mass losses that correspond to one bromine atom (calculated mass loss of 12% (**4**) and 13 (**5**) % respectively). An additional step (100−230 °C (**5**) involving 4%) is observed in case of **5** due to the solvent molecule cocrystallized (calculated 4%).

The thermal analysis of polymeric **2**, **6**, **7**, **9**, and **10** shows one-step decomposition (100−445 °C for **2**, 180−395 °C for **6**, 180−290 °C for **7**, 100−243 °C for **9**, and 100−425 °C for **10**) involving 75% (**2**), 79% (**6**), 83% (**7**), 81% (**9**), and 79% (**10**), respectively, which correspond to the simultaneous evolution of both two ligands and three bromine atoms (five bromine atoms in case of **10**) (calculated for 2 ligands and 3 Br (5 Br in case of **10**) 79% (**2**), 79% (**6**), 79% (**7**), 83% (**9**) and 79% (**10**), respectively). However, polymeric **1** and **8** are found to decompose in two steps. In the case of **1**, the first stage of decomposition (185−280 °C) involves 47% mass loss that corresponds to the evolution of three bromine atoms (calculated mass loss of 47%). The second stage of decomposition (280−350 °C) involves 28% mass loss that corresponds to the two ligands (calculated mass loss of 30%). In the case of **8**, the first stage of decomposition (100−210 °C) involves 13% mass loss that

corresponds to the evolution of one bromine atom (calculated mass loss of 13%). The second stage of decomposition (210−340 °C) involves 66% mass loss that corresponds to the two ligands (calculated mass loss of 66%).

Vibrational Spectroscopy. The IR spectra of the complexes show distinct vibrational bands at 1589−1460 and 1387−1219 cm^{-1}, which can be assigned to υ(CN) vibrations (thioamide I and II bands) and at 1185−990 cm^{-1} and 816−623 cm^{-1}, which can be attributed to the υ(CS) vibrations (thioamide III and IV bands).[11,12] Variations in the geometrical features of **1**−**10** (ionic salt O_h, dimer SP, or polymeric SP, see crystal structures) lead to variations in Sb−Br and/or Sb−S bond distances due to inter- and intramolecular interactions (crystal structures). Therefore, far-IR spectroscopy can be a very useful tool in the geometrical characterization of these complexes. The tentative assignment of the M−L vibrations are ionic salt O_h **3**, which shows one ν(Sb−Br) band at 228 cm^{-1}[13] and one ν(Sb−S) vibration band at 275 cm^{-1}.[13] The dimeric **4** and **5** with one bridging and one terminal bromine atom show $\nu(Sb-Br_{(bridging)})$ bands at 200 (**4**) and 213 (**5**) cm^{-1} and $\nu(Sb-Br_{(terminal)})$ bands at 212 (**4**) and 232 cm^{-1} (**5**),[13] whereas the ν(Sb−S) vibrations appear at 271 (**4**) and 273 (**5**) cm^{-1}.[13] The polymeric **7** and **8** with bridging μ_2-Br show $\nu(Sb-Br_{(bridging)})$ bands at 208 (**7**) and 200 (**8**) cm^{-1} and $\nu(Sb-Br_{(terminal)})$ bands at 228 (**7**) and 230 (**8**) cm^{-1},[13] whereas the ν(Sb−S) vibration appears at 281 (**7**) and 275 (**8**) cm^{-1}.[13] Polymeric **6** with μ_2-S shows a $\nu(Sb-S_{(bridging)})$ band at 275 cm^{-1} and a $\nu(Sb-S_{(terminal)})$ band at 282 cm^{-1},[13] whereas the ν(Sb−Br) band was observed at 209 cm^{-1}.[13] The polymeric ionic salt **10** with bridging μ_2-Br shows $\nu(Sb-Br_{(bridging)})$ bands at 213 cm^{-1} and $\nu(Sb-Br_{(terminal)})$ at 213 cm^{-1},[13] whereas the ν(Sb−S) vibration band appears at 273 cm^{-1}.[13] **1**, **2**, and **9** for which no structural data are available show ν(Sb−Br) bands at 222 and 199 cm^{-1} (**1**), 218 and 209 cm^{-1} (**2**), and 222 and 200 cm^{-1} (**9**)[13] and ν(Sb−S) vibration bands at 272 (**1**), 278 (**2**), and 270 (**9**) cm^{-1},[13] which classify them as either dimeric or polymeric types of complexes in agreement with TG-DTA data (above).

The [ν(Sb−S) and ν(Sb−Br)] stretching vibrations are also Raman active.[14] Thus, the Raman spectrum of the ionic salt **3**, with O_h geometry, shows vibrational bands at 259 and 198 cm^{-1}, which are assigned to the v(Sb−Br) and v(Sb−S), respectively.[14] Dimeric **4** and **5** with one bridging and one terminal bromine atom exhibit $\nu(Sb-Br_{(terminal)})$ bands at 241 cm^{-1} (**4**) and 256 (**5**) cm^{-1} and $\nu(Sb-Br_{(bridging)})$ bands at 216 (**5**) cm^{-1},[14] whereas the ν(Sb−S) bands appear at 194 (**4**) and 184 (**5**) cm^{-1}.[14] No $\nu(Sb-Br_{(bridging)})$ band was observed in the case of **4**. Polymeric **6** with μ_2-S displays $\nu(Sb-S_{(bridging)})$ at 181 cm^{-1} and a $\nu(Sb-S_{(terminal)})$ band at 197 cm^{-1},[14] whereas the ν(Sb−Br) band is observed at 261 cm^{-1}.[14] Polymeric **8** with bridging shows only one ν(Sb−Br) band at 220 cm^{-1}, whereas the ν(Sb−S) vibration appears at 182 cm^{-1}.[14] **1** and **2** where no structural data are available show ν(Sb−Br) bands at 245 and 217 cm^{-1} (**1**) and at 251 cm^{-1} (**2**)[14] and ν(Sb−S) vibration bands at 193 cm^{-1} (**1**) and 199 (**2**) cm^{-1},[14] which lead them to be classified as either dimeric or polymeric complexes.

Conductivity Measurements. The influence of solvent media on the complex geometries was studied by measuring the molar conductance at 25 °C. In methanol, the complexes exhibit molar conductances values of 174 (**1**), 212 (**2**), 254 (**3**), 213 (**4**), 216 (**5**), 212 (**6**), 315 (**7**), 197 (**8**), 212 (**9**), and 339 (**10**) cm^{-1} mol^{-1} Ω^{-1}, respectively. In acetonitrile on the other hand, the molar conductances measured for **1**, **2**, and **4**−**9** were 25 (**1**), 11 (**2**), 11 (**4**), 5 (**5**), 16 (**6**), 41 (**7**), 3 (**8**), 5 (**9**), and 101 (**10**) cm^{-1} mol^{-1} Ω^{-1}, respectively, which correspond to nonionic configurations, as expected (crystal structures). In case of **3**, however, a molar conductance value of 75 cm^{-1} mol^{-1} Ω^{-1} was initially measured due to the presence of two ions for this complex, which ends up to 27 cm^{-1} mol^{-1} Ω^{-1} and corresponds to a nonionic compound. La Manna et.al.[15] on the basis of conductivity measurements proposed that the equilibrium shown in eq V was established for antimony(III) halides in methanolic solutions. Recently, we also reported an equilibrium between ionic O_h and nonionic (SP) complexes[11] (eq VI). Because the formation mechanism of the ionic salt complexes with O_h geometry involves the Sb−Br bond cleavage (X-ray structure), such types of complexes might form through the [$SbBr_2^+$] species and only in methanol. In acetonitrile solutions, the compounds are neutral and so only polymeric or dimeric Ψ-O_h complexes could be formed. The ΔG of the reaction (eq V) was calculated to be −102.1 and −100.3 kcal/mol in water and methanol solutions respectively, in favor of this equilibrium (Computational Studies).

$$2SbBr_3 \rightleftharpoons SbBr_4^- + SbBr_2^+ \qquad \text{(V)}$$

$$2SbCl_3L_2 \rightleftharpoons [SbL_4Cl_2]^+Cl^- + SbCl_3 \qquad \text{(VI)}$$

Crystal and Molecular Structures of {[$SbBr_2$(MBZIM)$_4$]$^+$ [Br]$^-$ H_2O} (3), {[$SbBr_2$(μ_2-Br)(MMBZIM)$_2$]$_2$} (4), {[$SbBr_2$(μ_2-Br)(EtMBZIM)$_2$]$_2$ MeOH} (5), {[$SbBr_3$(μ_2-*S*-tHPMT)(tHPMT)]$_n$} (6), {[$SbBr_2$(μ_2-Br)(PYT)$_2$]$_n$} (7), {[$SbBr_2$(μ_2-Br)(MTZD)$_2$]$_n$} (8), and {[$SbBr_5$]$^{2-}$[($PMTH_2^+$)$_2$]} (10). Crystal structures of antimony(III) bromide compounds are very rare in the literature (see Introduction). Until now antimony(III) bromide complexes with thione/thiole were found to adopt octahedral (O_h)[8a] and pseudotrigonal-bipyramidal (**Ψ-TBP**)[8b−d] geometries (Scheme 1).

ORTEP diagrams of **3**, **4**, **5**, **6**, **7**, **8**, and **10** are shown in Figures 1−7, whereas selected bond lengths and angles are given in Table 1.

3, synthesized in methanol/dichloromethane (1:1) solutions, is a monomeric ionic salt in the solid state and it is

(12) (a) Daga, V.; Hadjikakou, S. K.; Hadjiliadis, N.; Kubicki, M.; dos Santos, J. H. Z.; Butler, I. S. *Eur. J. Inorg. Chem.* **2002**, *1718*, 1728. (b) Zachariadis, P. C.; Hadjikakou, S. K.; Hadjiliadis, N.; Michaelidis, A.; Skoulika, S.; Balzarini, J.; De Clercq, S. *Eur. J. Inorg. Chem.* **2004**, *1420*, 1426. (c) Hadjikakou, S.; Antoniadis, C. D.; Hadjiliadis, N.; Kubicki, M.; Binolis, J.; Karkabounas, S. *Inorg. Chim. Acta* **2005**, *358*, 2861–2866.

(13) Williams, J. D.; Viehbeck, A. *Inorg. Chem.* **1979**, *18*, 1823–1825.

(14) (a) Ludwig, C.; Dolny, M.; Gotze, H.-J. *Spectrochim. Acta, Part A* **2000**, *56*, 547–555. (b) Lu, S. F.; Huang, J. Q.; Huang, X. Y.; Wu, Q. J.; Yu, R. M. *Inorg. Chem.* **1999**, *38*, 3801–3805.

(15) La Manna, G.; Turco Liveri, M. L.; Liveri, V. T.; Saiano, F.; Alonzo, G. *J. Solution Chem.* **1993**, *22*, 1063–1071.

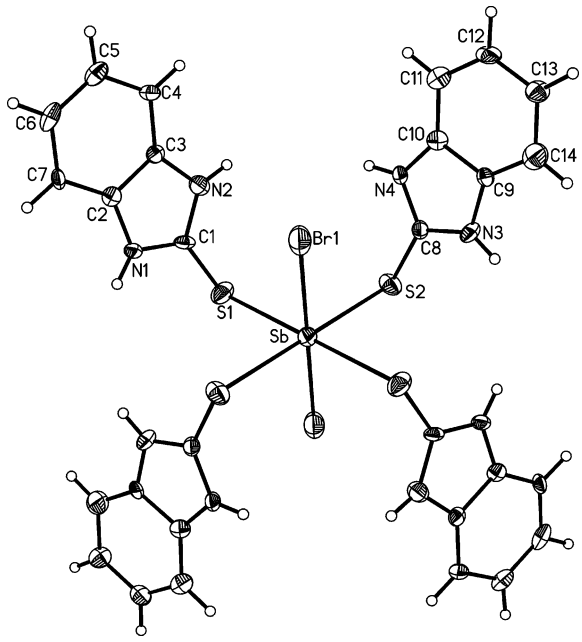

Figure 1. Anisotropic ellipsoid representation of **3**. The ellipsoids are drawn at 50% probability level. The unlabeled part of the molecule is generated by the symmetry operation $1 - x, -y, -z$.

the first example of an ionic antimony(III) bromide compound with octahedral (O_h) geometry. Four sulfur atoms from thione ligands and two bromide ions form an octahedral (O_h) cationic $[SbS_4Br_2]^+$ cation in which the two bromide anions occupy axial positions. A third bromide counteranion neutralizes the whole complex. **3** and the corresponding ones with $SbCl_3$ with MBZIM, $\{[SbCl_2(MBZIM)_4]^+ \cdot Cl^- \cdot 2H_2O \cdot (CH_3OH)\}$, $\{[SbCl_2(MBZIM)_4]^+ \cdot Cl^- \cdot 3H_2O \cdot (CH_3CN)\}$[11] are similar species of a new class of Sb compounds.

4 and **5** are dimers, whereas **6**, **7**, and **8** are polymers, built up from monomeric units with square pyramidal (SP) geometries around the metal center. Two sulfur atoms from thioamide ligands and three bromine atoms, bound to Sb atoms formed the building blocks of the dimers and polymers. Strong intramolecular interactions between μ_2-Br (**4**, **5**, **7**, and **8**) or μ_2-S (**6**) and Sb atoms lead to dimeric (**4** and **5**) or to polymeric (**6**, **7**, and **8**) assemblies with pseudooctahedral (Ψ-O_h) geometries around the Sb(III) ion.

The equatorial plane in both SP units of the dimeric **4** and **5** is formed by two Br and two S atoms in a *trans*-S, *trans*-Br arrangement. Two strong intramolecular μ_2-Br···Sb interactions (3.266 Å (**4**) and 3.203 Å (**5**)) complete the Ψ-O_h geometry leading to the dimeric **4** and **5**. Because the sum of van der Waals radii for Sb−Br bonds is 4.10−4.51 Å,[16] the μ_2-Br···Sb interaction can be considered as strong. The equatorial plane in the SP unit of the polymeric **6** is formed by three Br and one S atom in *b*,*c*,*d*-Br arrangement. An additional strong intramolecular μ_2-S···Sb interaction (3.221 Å shorter than the sum of van der Waals radii (4.0−4.47 Å)[16]) completes the Ψ-O_h geometry forming a 1D zigzag polymeric **6**. The equatorial plane in the SP unit of the polymeric **7** is formed by three Br and one S atoms in a *b*,*c*,*d*-Br arrangement, whereas μ_2-Br···Sb conducts (3.417 and 3.069 Å) complete the Ψ-O_h geometry leading to the 1D polymer **7** with helical conformation. Finally, the equatorial plane in the SP unit of the polymeric **8** is formed by two S and two Br atoms in a *cis*-S, *cis*-Br arrangement, whereas a weaker μ_2-Br···Sb contact (3.742 Å) completes the Ψ-O_h geometry leading to the 1D zigzag polymer **8**.

It is therefore clear that the arrangements around the metal center of these antimony(III)−thione complexes are octahedral (O_h) or pseudo-octahedral (Ψ-O_h). In methanolic or water solutions on the other hand, MBZIM forms the ionic salt **3** ($\{[SbBr_2(MBZIM)_4]^+ [Br]^- H_2O\}$) with O_h geometry most probably through the $[SbBr_2^+]$ species.

The complexes of the other thioamide ligands studied here include dimers (**4** and **5**) or polymers (**6**, **7**, and **8**) with monomeric units of square pyramidal (SP) geometries around the metal center as building blocks. Strong intramolecular interactions between μ_2-Br (**4**, **5**, **7**, and **8**) or μ_2-S (**6**) and Sb atoms lead to dimeric (**4** and **5**) or to polymeric (**6**, **7** and **8**) assemblies with pseudooctahedral (Ψ-O_h) geometries around the Sb(III) ion. Thus, *trans*-S, *trans*-Br SP units lead to dimers (**4** and **5**) with two μ_2-Br interactions. *cis*-S and *cis*-Br SP stereoisomers lead to zigzag polymeric assemblies of $\{[SbBr_2(\mu_2\text{-Br})(MTZD)_2]_n\}$ building blocks through μ_2-Br interactions (**8**). Complexes of *b*,*c*,*d*-Br SP units are polymers with either zigzag (**6**) through μ_2-S bridges or helical (**7**) through μ_2-Br bridges assemblies. The structural differences in the bridging atom (μ_2-Br or μ_2-S) observed between **6** and **7**−**8** might be due to (i) the charge of the bridging atom or (ii) the electron donor capacity between μ_2-Br and μ_2-S because Sb(III) is known to be an acid of intermediate strength preferring intermediate bases as ligands for complex formation (Computational Study). In case of **7**with helical structure, the dihedral $Sb{-}X_{bridging}{\cdots}Sb'{-}X'_{bridging}$ angle is −37.48°, whereas in **6** and **8** with zigzag polymeric structures these angles are −168.69° (**6**) and −152.96° (**8**), respectively (Figures 4 and 6).

The Sb−S bond distances varied from 2.514(3) (**7**) to 2.8427(7) (**8**) Å (Table 1) in **3**−**8** and **10**, with the longest found in **8**. The Sb−S distances in $\{[SbCl_2(MBZIM)_4]^+ \cdot Cl^- \cdot 2H_2O \cdot (CH_3OH)\}$, $\{[SbCl_2(MBZIM)_4]^+ \cdot Cl^- \cdot 3H_2O \cdot (CH_3CN)\}$. *a*,*b*,*c*-Cl $[SbCl_3(MBZIM)_2]$, *a*,*b*,*d*-Cl $[SbCl_3(EtMBZIM)_2]$, *a*,*b*,*c*-Cl $[SbCl_3(MTZD)_2]$, and *b*,*c*,*d*-Cl $[SbCl_3(tHPMT)_2]$[11] varied from 2.482 to 2.849 Å.[11] The Sb−Br bond distances in **3**−**8** and **10** lie between 2.537(3) (**8**) and 3.0685(14) (**7**) Å (Table 1). The Sb−Br bond lengths are in agreement with the corresponding bond distances found in $[Sb(k^3\text{-}Tm^{Me})(k^1\text{-}Tm^{Me})Br]$ (Tm^{Me} = hydrotris(methimazolyl)borate) 2.9163(5) Å,[8a] $[SbBr(dmit)(THF)]_n$ (dmit = 2-thioxo-1,3-dithiole-4,5-dithiolato) 2.5833(3) Å,[8b] {[Ph−CH═CH(Ph)S]SbBr} 2.505(1) Å,[8c] and $[S(C_6H_4S)_2]SbBr$ 2.6373(6) Å.[8d]

The C−S bond lengths in the case of **3**−**8** and **10** varied from 1.676(18) to 1.761(3) Å, supporting the ligand coordination through their thionate forms (average C−S = 1.69 Å).[11]

Although the axial Br−Sb−Br and the basal S1−Sb−S1a and S2−Sb−S2a angles are 180°, the corresponding basal S1−Sb−S2 and S1a−Sb−S2a angles are different that 90°,

(16) (a) Batsanov, S. S. *Inorg. Mater.* **2001**, *37*, 871–885. Translated from Neorganicheskie Materialy, **2001**, *37*, 1031−1046. (b) Bondi, A. *J. Phys. Chem.* **1964**, *68*, 421–451.

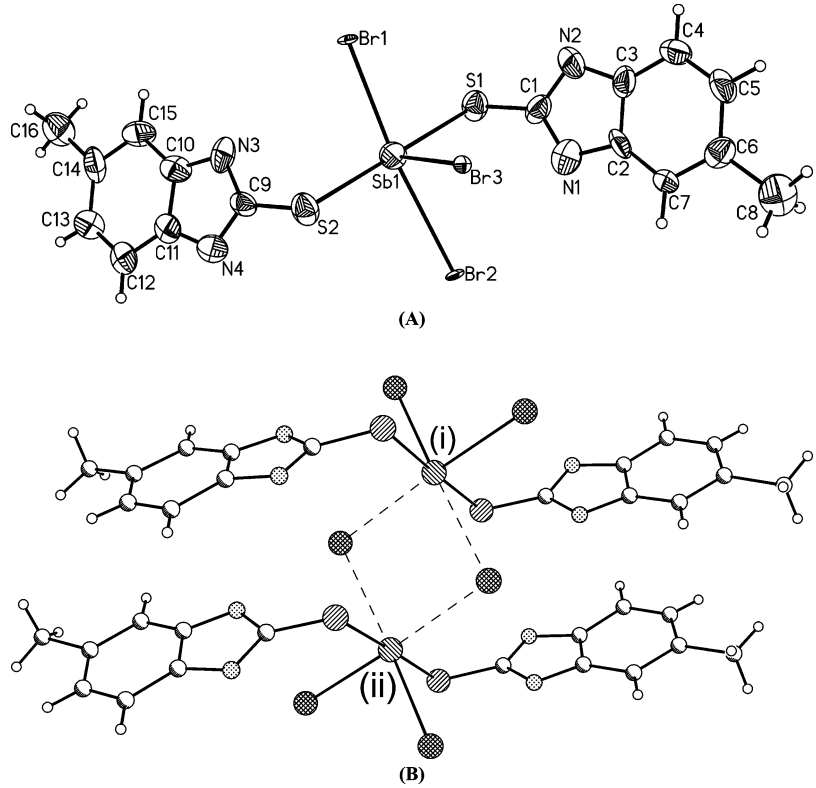

Figure 2. (A) Anisotropic ellipsoid representation of the building block of **4** with *trans*-Br, *trans*-S SP conformation. The ellipsoids are drawn at 50% probability level. The counteranion is omitted for clarity (Experimental Section). (B) Strong intramolecular μ_2-Br···Sb interactions lead to dimerization with Ψ-O_h geometry around Sb center. Symmetry codes: (i) x, y, z; (ii) $2 - x$, $-y$, $-z$.

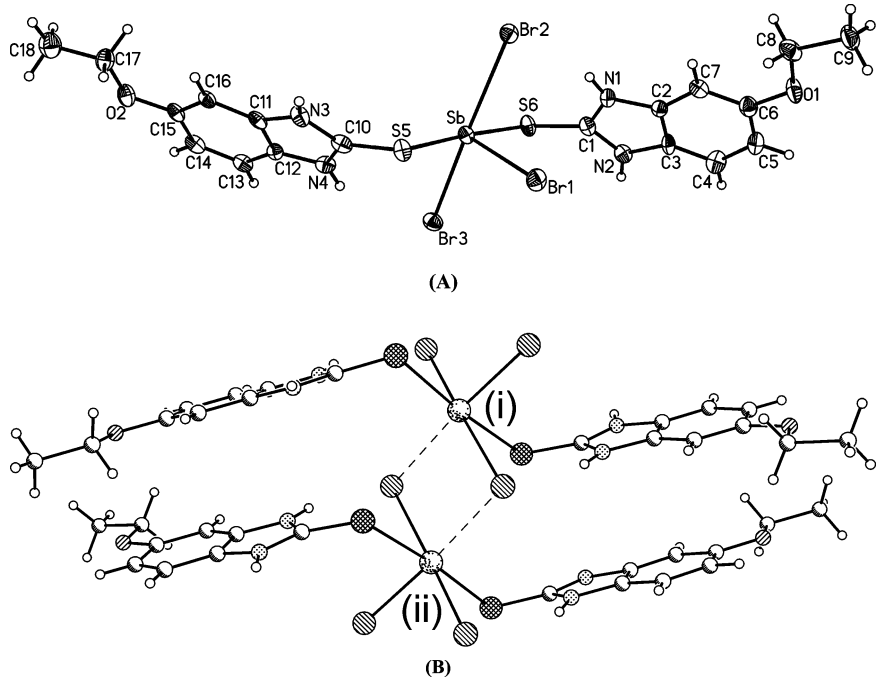

Figure 3. (A) Anisotropic ellipsoid representation of the building block of **5** with *trans*-Br, *trans*-S SP conformation. The ellipsoids are drawn at 50% probability level. (B) Strong intramolecular μ_2-Br···Sb interactions lead to dimerization with Ψ-O_h geometry around Sb center. Symmetry codes: (i) x, y, z; (ii) $-x$, $-y$, $1 - z$.

and therefore the geometry is a distorted octahedron. The lone pair of electrons located on the Sb atom in **4**−**8** affects the ideal SP geometries around the metal ion[17,18] because the basal bond angles are found to vary from the ideal values of 180° or 90° (Table 1) as expected from the valance shell electron pair repulsion theory (VSEPR) (Br1−Sb1−S1 = 88.28(13)° and Br2−Sb1−Br1 = 172.8(1)° in **4** (Figure 2), Br2−Sb1−S5 = 82.49(3)° and Br2−Sb1−Br3 = 177.76(2)°

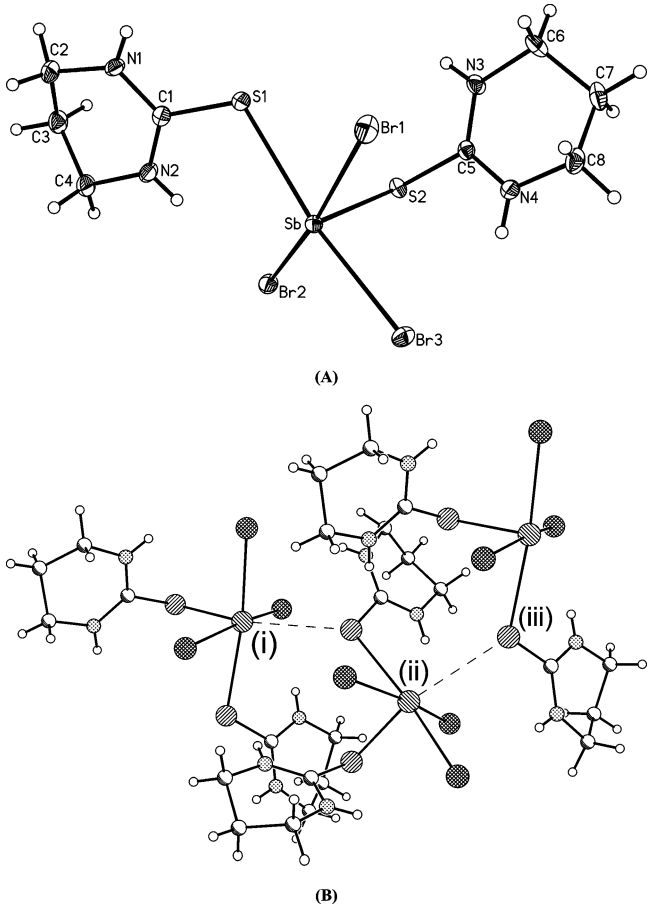

Figure 4. (A) Anisotropic ellipsoid representation of the building block of **6** with *b*,*c*,*d*-Br SP conformation. The ellipsoids are drawn at 50% probability level. (B) Strong intramolecular μ_2-S···Sb interactions lead to zigzag polymerization with Ψ-O_h geometry around Sb center. Symmetry codes: (i) x, y, z; (ii) $x, {}^1/_2 - y, {}^1/_2 + z$; (iii) $x, y, 1 + z$.

in **5** (Figure 3), Br1−Sb1−Br3 = 92.97(1)° and Br1−Sb1−Br2 = 165.33(1)° in **6** (Figure 4), Br1−Sb1−Br2 = 165.39(5)° and Br1−Sb1−S12 = 79.54(10)° in **7** (Figure 5) and Br3−Sb1−S2 = 170.35(2)° and Br2−Sb1−S2 = 88.74(2)° in **8** (Figure 6).

10 is a polymeric ionic salt compound in the solid state, and it is the first example of a new category of antimony(III) compounds. Five bromide ions form a dianionic $[SbBr_5]^{2-}$ counterion with SP geometry around Sb(III) Sb−Br bond distance varied between 2.57−2.26 Å. One bridging μ_2-Br atom from a sequential $[SbBr_5]^{2-}$ unit complete the octahedron around the metal center. The (Sb-(μ_2-Br) is found to be 3.194 Å, whereas the basal angles are almost 90° (Table 1) confirming the octahedral arrangement. The compound is neutralized by two protonated $PMTH_2^+$ ligands.

X-ray Powder Diffraction Study. To examine further our hypothesis about the influence of water or methanol on the geometry adopted by the Sb(III) complexes (conductivity measurements) we studied the X-ray powder diffraction (XRPD) spectra of **3** (calculated from single crystal X-ray diffraction pattern (**A**), before and after heating at 110 °C for 2 h (**B** and **C**), and the one after rehydration (**D**) (Figure 8). The XRPD diagrams showed that removing a water molecule from the initial sample (**B**) led to the crystal lattice (**C**). These produce (**D**) following rehydration of (**C**), identical to the initial (**B**). The lattice (**C**) may correspond to an SP geometry as in the case of chloride analogs of the same complexes,[11] whereas (**B**) and (**D**) adopt an O_h geometry. Finally, a similar behavior was also observed by Giolando et al.[19] with O_2 influencing the geometry of the $\{[Sb^V(1,2\text{-}S_2C_6H_4)_3]^-\}$ complex in a similar fashion.

Computational Study. To investigate further the factors governing the geometry of antimony(III) thione complexes (crystal structures) we performed computational studies by means of density functional theory (DFT) with Becke3-LYP method using standard basis sets 6-31G(d) (Table 2).

Thus, in methanolic or water media the ionic salt **3** with O_h geometry was formed, in the case of the MBZIM ligand, most probably through the $[SbBr_2^+]$ species (eq V).The ΔG of eq V is −102.1 or −100.3 Kcal/mol in water or methanol, respectively.

Other thioamide ligands studied here form dimers or zigzag and helical polymer complexes that are built up from SP units. In these cases, either μ_2-Br or μ_2-S bridges were observed. The partial negative charges on sulfur atoms were calculated for the thiones used in this work and the results are shown in Table 2. They are summarized as: (i) The higher negative charge on the sulfur atom (−0.45 e), lower HOMO energy, which is related with its basicity[20a] (−0.3448 hartree) and higher nucleophilicity[20b] (−0.3556 hartree) forms zigzag polymeric conformation with μ_2-S bridges in the case of the tHPMT complex. (ii) Ligands with lower negative charges on their sulfur atoms, on the other hand, with lower basicity and lower nucleophilicity yield polymers with μ_2-Br bridges. Thus, the PYT and MTZD ligands with lower sulfur charge (−0.38 e (PYT) and −0.31 e (MTZD)), lower basicity (−0.2028 and −0.2162 hartree for PYT and MTZD, respectively), and lower nucleophilicities (−0.1470 hartree (PYT) and −0.1853 hartree (MTZD)) (Table 2)) afford polymeric complexes with helical (**7**) and zizag (**8**) conformations through μ_2-Br bridges. (iii) Ligands with similar negative charges on their sulfur atoms and lower bacicity and nucleophilicity form dimers. Thus, sulfur charges of −0.37 e in case of MMBZIM ligand and −0.38 e for EtMBZIM and more lower HOMO energies (basicity) (−0.1994 and −0.1928 hartree for MMBZIM and EtMBZIM) and nulceophilicities of −0.1725 and −0.1694 hartree for MMBZIM and EtMBZIM respectively (Table 2) lead to dimers with μ_2-Br bridges (**4** and **5**). This result may be attributed to steric reasons in case of the trans isomers where the formation of dimers allowed by their general arrangements stops the reaction and polymers cannot form for **1**, **2**, and **9** where structural data are not available yet; the computational studies indicate polymeric assemblies for **1** and **2** most probably with μ_2-S bridges and a dimeric conformation with the μ_2-Br bridge in the case of **9** (Table 2).

(17) (a) Haiduc, I.; Silvestru, C. *Main Group Elements and Their Compounds*; Springer-Verlag: Berlin, 1996; p 355. (b) Liu, Y; Tiekink, E. R. T. *CrystEngComm* **2005**, *7*, 20–27.

(18) Vickaryous, W. J.; Zakharov, L. N.; Johnson, D. W. *Main Group Met. Chem.* **2006**, *5*, 51–59.

(19) Wegener, J.; Kirschbaum, K; Giolando, D. M. *J. Chem. Soc., Dalton Trans.* **1994**, *121*, 3–1218.

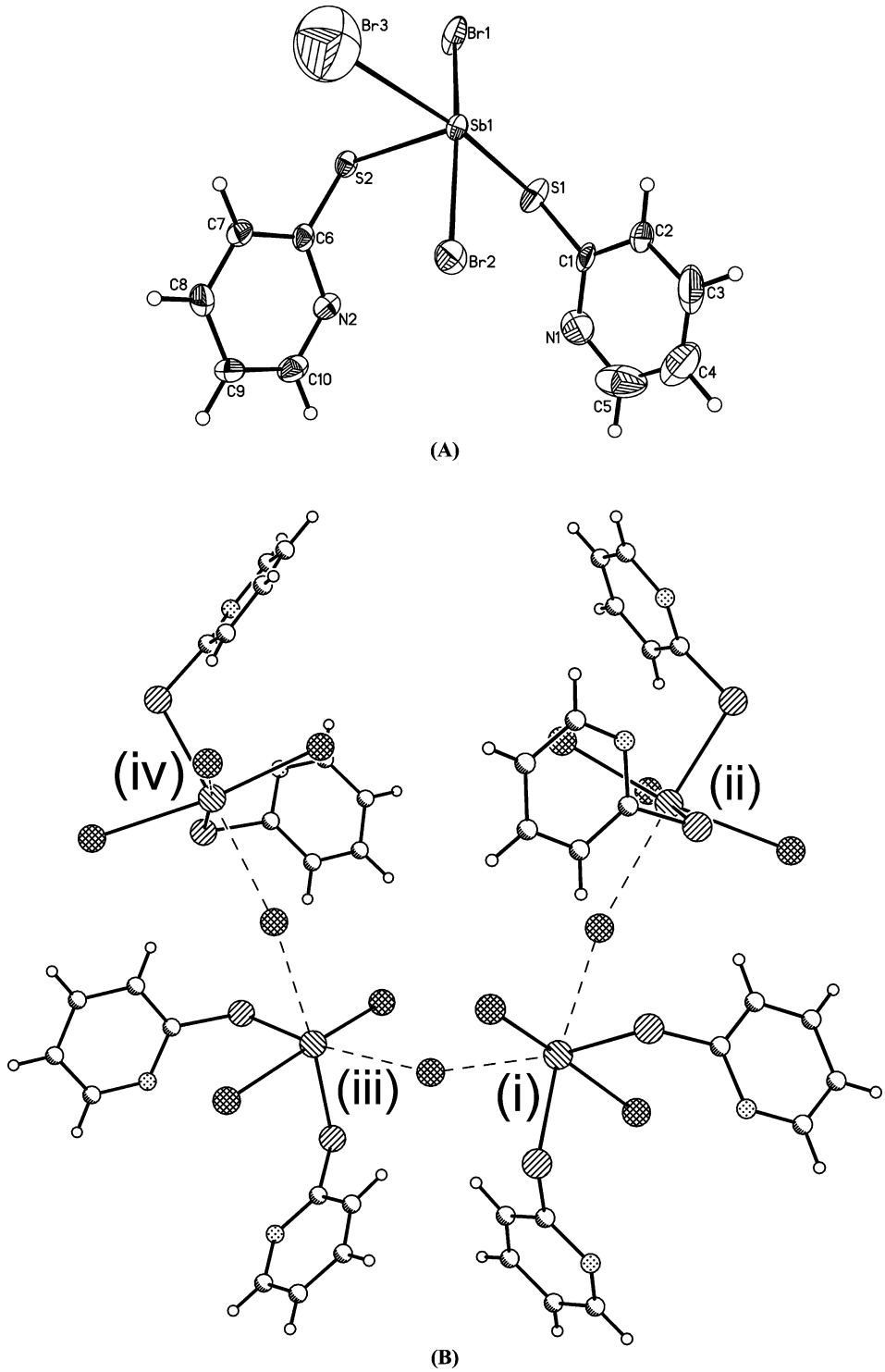

Figure 5. (A) Anisotropic ellipsoid representation of the building block of **7** with *b*,*c*,*d*-Br SP conformation. The ellipsoids are drawn at 50% probability level. The strange shape of Br3 ellipsoid is probably the result of the disorder (text). (B) Strong intramolecular μ_2-Br···Sb interactions lead to helicoidal polymerization with Ψ-O_h geometry around Sb center. Symmetry codes: (i) x, y, z; (ii) $2 - x, y, {}^1/_2 - z$; (iii) ${}^5/_2 - x, -y, z$; (iv) ${}^1/_2 + x, -y, {}^1/_2 - z$.

Biological Tests. Cytostatic Activity. 1−10 were evaluated in vitro for their inhibitory effects on the proliferation of murine leukemia cells (L1210), murine mammary carcinoma cells (FM3A), human T-lymphocyte cells (Molt4/C8, CEM) and human cervix carcinoma cells (HeLa). The results of this study are reported, as 50% inhibitory concentration (IC_{50}) values in Table 3. The corresponding IC_{50} values of the cytotoxic activity of the Sb **1−10** toward lung embryonic fibroblasts (Hel) cells and their concentrations required to cause visible alterations in 50% of intact Hel cells are also reported in Table 3. Complexes **1−10** showed usually a modest cytostatic activity against the tumor cell lines studied (Table 3). Antimony(III) bromide−thione complexes consistently showed a more selective antiproliferative activity against HeLa cells, which also observed in case of the corre-

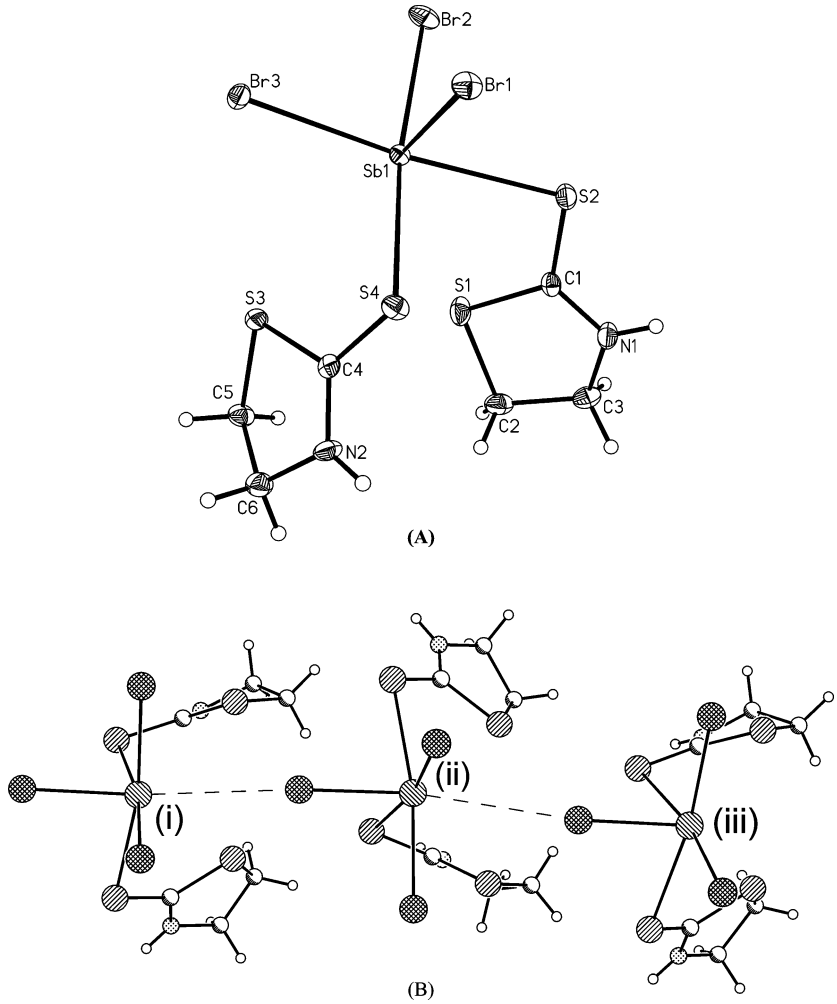

Figure 6. (A) Anisotropic ellipsoid representation of the building block of **8** with *cis*-Br, *cis*-S SP conformation. The ellipsoids are drawn at 50% probability level. (B) Strong intramolecular μ_2-Br···Sb interactions lead to zigzag polymerization with Ψ-O_h geometry around the Sb center. Symmetry codes: (i) *x*, *y*, *z*; (ii) *x*, $^1/_2 - y$, $^1/_2 + z$; (iii) *x*, *y*, $1 + z$.

sponding antimony(III) chloride complexes studied previously[11] (Table 3). However, the antimony(III) bromide complexes studied here were at the average less active than the corresponding chlorides studied previously (Table 3).[11] The antiproliferative activity against cervix carcinoma (HeLa) cells was 2−3 to >10-fold more potent than against the leukemia and lymphocyte cells. Polymeric ionic **10** with O_h geometry around the metal center exhibits a slightly stronger cytotoxicity against murine leukemia cells (L1210), murine mammary carcinoma cells (FM3A), T-lymphocyte cells (Molt4/C8, CEM), and human cervix carcinoma cells (HeLa). The corresponding IC_{50} values found for cisplatin and carboplatin on the proliferation of HeLa cells are 10 and >37 μM (3.0 and >11 μg/ml), respectively.[20a] Thus, all antimony(III) **1**−**10** tested showed comparable activity against the cervix carcinoma HeLa cells, whereas the cytotoxicity of **10** is 3−4 times higher than that of carboplatin.[20a] The IC_{50} values found for cisplatin on the proliferation of L1210 or Molt4 cells are 0.23 and 0.33 μM (0.07 and 0.1 μg/ml),[20b,22b] respectively, indicating low cytotoxic activity of **1**−**10** against these cell lines in respect to cisplatin.

Conclusions

The conclusions drawn from the above work are: (i) the geometries around antimony(III) are found to be either octahedral (O_h) or pseudo-octahedral (Ψ-O_h). Thus, the O_h geometry in case of the ionic salt **3** is achieved, most probably through ionization, as shown in eqs V and VI, producing the [$SbBr_2^+$] species. This assembly is found to depend solely on solvent media.[11] The other thioamide ligands studied here produce dimers (**4** and **5**) or polymers

(20) (a) I. Fleming, *Frontier Orbitals and Organic Reactions*; Wiley: Londo, 1976; *183*−*190*, pp 35−40. (b) Hemmateenejad, B.; Safarpour, M. A.; Taghavi, F. *J. Mol. Struct. (Theochem)* **2003**, 635.

(21) (a) Carland, M.; Tan, K. J.; White, J. M.; Stephenson, J.; Murray, V.; Denny, W. A.; McFadyen, D. *J. Inorg. Biochem.* **2005**, *99*, 1738–1743. (b) Shamsuddin, S.; Takahashi, I.; Siddik, Z. H.; Khokhar, A. R. *J. Inorg. Biochem.* **1996**, *61*, 291–301. (c) Dabholkar, M.; Parker, R.; Reed, E. *Mutat. Res.* **1992**, *274*, 45–56.

(22) (a) *Oxford Diffraction, CRYSALIS CCD and CRYSALIS RED*, version p171.29.2; Oxford Diffraction Ltd.: Abingdon, Oxford, England, 2006. (b) *CrysAlis CCD*, version 1.171.31.5; Oxford Diffraction Ltd. (release 28−08−2006 CrysAlis171.NET). (c) *CrysAlis RED*, version 1.171.31.5; Oxford Diffraction Ltd. (release 28−08−2006 CrysAlis171.NET). (d) Sheldrick, G. M. *Acta Crystallogr.* **1990**, *A46*, 467. (e) Sheldrick, G. M. *SHELXL-97, Program for the Refinement of Crystal Structures*, University of Göttingen: Göttingen, Germany, 1997.

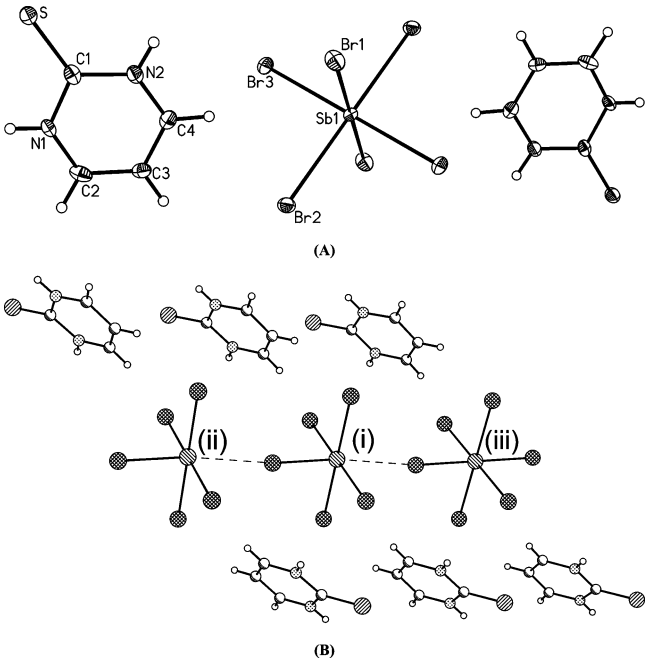

Figure 7. (A) Anisotropic ellipsoid representation of the building block of **10**. The ellipsoids are drawn at 50% probability level. The unlabeled part of the molecule is generated by the symmetry operation $-x, -y, 1 - z$. (B) Strong intramolecular μ_2-Br···Sb interactions lead to 1D polymerization with Ψ-O_h geometry around Sb center. For clarity, only one of the two disordered μ_2-Br atoms (with 0.5 occupancy) is shown. Symmetry codes: (i) x, y, z; (ii) $1 + x, y, z$; (iii) $-1 + x, y, z$.

(**6**, **7**, and **8**), containing SP building blocks. In these cases, either μ_2-Br or μ_2-S bridges were observed. Strong intramolecular interactions between μ_2-Br (**4**, **5**, **7**, and **8**) or μ_2-S (**6**) and Sb atoms lead to dimeric (**4** and **5**) or polymeric (**6**, **7**, and **8**) assemblies with pseudooctahedral (Ψ-O_h) geometries around the Sb(III) ion. Thus, *trans*-S, *trans*-Br, and SP units lead to dimers (**4** and **5**) through two μ_2-Br interactions. *cis*-S, *cis*-Br, and SP stereoisomers lead to zigzag polymeric assemblies through μ_2-Br interactions (**8**). Complexes of *b*,*c*,*d*-Br SP units built up polymers with either zigzag (**6**) (through μ_2-S bridges) or helical (**7**) (through μ_2-Br bridges) assemblies. Crystallographic and computational data suggest that the differences in the bridging atoms (μ_2-Br or μ_2-S) observed between **6** and **7**−**8** might be due to (i) the charge of the bridging atom with the higher negatively charged atom (Br or S) to bridge the Sb units and (ii) the relative basicity between μ_2-Br and μ_2-S because Sb(III) in terms of Pearson's hard and soft acid and base approach is known to be an intermediate acid preferring to be bound to intermediate bases as ligands in forming complexes.

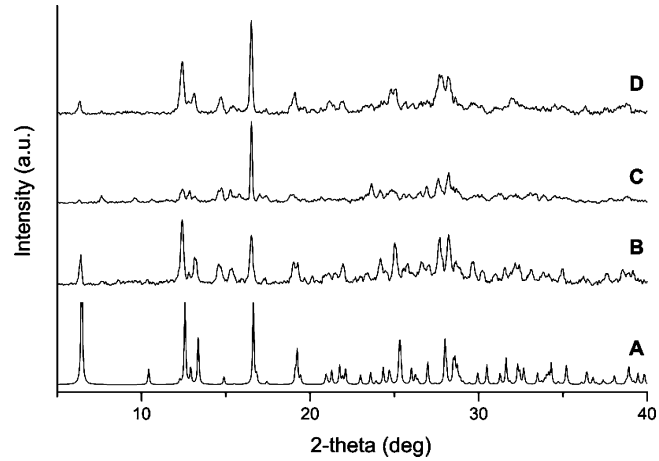

Figure 8. X-ray powder diffraction (XRPD) diagrams of **3** (calculated from single crystal X-ray diffraction pattern **A**) before and after heating at 110 °C for 2 h (**B** and **C**) and the one after rehydration (**D**).

The complexes showed moderate cytostatic activity against several tumor cell lines with preference for human cervix carcinoma (HeLa) cells as also observed in case of the corresponding antimony chloride complexes.[11]

Experimental Section

Materials and Instruments. All solvents used were of reagent grade. Antimony(III) bromide (Aldrich) as well as thiones thiourea (Aldrich), 2-mercapto-1-methylimidazole (Sigma), 2-mercaptobenzimidazole (Merck), 2-mercapto-5-methylbenzimodazole (Aldrich), 5-ethoxy-2-mercapto benzimidazole (Aldrich), 2-mercapto-3,4,5,6-tetrahydro-pyrimidine (Aldrich), 2-mercaptopyridine (Fluka), 2-mercaptothiazolidine (Aldrich), 3-methyl-2-benzothiazolinthion (Aldrich), and 2-mercaptopyrimidine (Aldrich) were used without further purification. Elemental analyses for C, H, N, and S were carried out with a Carlo Erba EA MODEL 1108 elemental analyzer. Melting points were measured in open tubes with a STUART scientific apparatus and are uncorrected. Infrared spectra in the region of 4000−370 cm^{-1} were obtained for KBr pellets, whereas far-infrared spectra in the region of 400−50 cm^{-1} were measured for polyethylene discs, with a PerkinElmer Spectrum GX FTIR spectrometer. Micro Raman spectra (64 scans) were recorded at room temperature using a low-power (∼30 mW) green (514.5) mm laser on a Renishaw In Via spectrometer set at 2.0 resolution. Thermal studies were carried out on a Shimadzu DTG-60 simultaneous DTA-TG apparatus, under a N2 flow (50 cm^3 min^{-1}) at a heating rate of 10 °C min^{-1}. Conductivity titrations were performed out at $T = 293$ K in methanol and acetonitrile or acetonitrile/water solutions with a WTF LF-91 conductivity meter.

Synthesis and Crystallization of $[SbBr_3(TU)_2]$ (1), $[SbBr_3(MMI)_2]$ (2), $\{[SbBr_2(MBZIM)_4]^+ [Br]^- H_2O\}$ (3), $\{[SbBr_2(\mu_2\text{-Br})(MMBZIM)_2]_2\}$ (4), $\{[SbBr_2(\mu_2\text{-Br})(EtMBZIM)_2]_2 MeOH\}$ (5), $\{[SbBr_3(\mu_2\text{-S-tHPMT})(tHPMT)]_n\}$ (6), $\{[SbBr_2(\mu_2\text{-Br})(PYT)_2]_n\}$ (7), $\{[SbBr_2(\mu_2\text{-Br})(MTZD)_2]_n\}$ (8), $[SbBr_3(MMBZT)_2]$ (9), and $[SbBr_3(PMT)]$ (10). 2-mercapto-benzimidazole (0.5 mmol, 0.075 g), 1.0 mmol of thiourea (0.076 g), 1.0 mmol of 2-mercapto-1-methylimidazole (0.114 g), 1.0 mmol of 2-mercapto-5-methylbenzimidazole (0.164 g), 1.0 mmol of 5-ethoxy-2-mercaptobenzimidazole (0,194 g), 1.0 mmol of 2-mercapto-

(23) (a) Becke, A. D. *Phys. Rev. A* **1988**, *38*, 3098–3100. (b) Becke, A. D. *J. Chem. Phys.* **1993**, *98*, 5648–5652. (c) Lee, C.; Yang, W.; Parr, R. G. *Phys. Rev. B* **1988**, *37*, 785–789. (d) Stephens, P. J.; Devlin, F, J; Chabalowski, C. F.; Frisch, M. J. *J. Phys. Chem.* **1994**, *98*, 1162311 627. (e) Hehre, W. J.; Ditchfield, R; Pople, J. A. *J. Chem. Phys.* **1972**, *56*, 2257–2261. (f) Frisch, M. J.; Pople, J A; Binkley, J. S. *J. Chem. Phys.* **1984**, *80*, 3265–3269. (g) Frisch, M. J.; Trucks, G. W.; Schlegel, H. B.; Scuseria, G. E.; Robb, M. A.; Cheeseman, J. R.; Zakrzewski, V. G.; Montgomery, J. A., Jr.; Stratmann, R. E.; Burant, J. C.; Dapprich, S.; Millam, J. M.; Daniels, A. D.; Kudin, K. N.; Strain, M. C.; Farkas, O.; Tomasi, J.; Barone, V.; Cossi, M.; Cammi, R.; Mennucci, B.; Pomelli, C.; Adamo, C.; Clifford, S.; Ochterski, J.; Petersson, G. A.; Ayala, P. Y.; Cui, Q.; Morokuma, K.; Malick, D. K.; Rabuck, A. D.; Raghavachari, K.; Foresman, J. B.; Cioslowski, J.; Ortiz, J. V.; Stefanov, B. B.; Liu, G.; Liashenko, A.; Piskorz, P.; Komaromi, I.; Gomperts, R.; Martin, R. L.; Fox, D. J.; Keith, T.; Al-Laham, M. A.; Peng, C. Y.; Nanayakkara, A.; Gonzalez, C.; Challacombe, M.; Gill, P. M. W.; Johnson, B.; Chen, W.; Wong, M. W.; Andreas, J. L.; Gonzalez, C.; Head-Gordon, M.; Replogle, E. S.; Pople, J. A. *Gaussian 98*; Gaussian: Pittsburgh, PA, 1998.

Table 1. Selected Bond Lengths (Angstroms) and Angles (Degrees) for Antimony(III) Bromide **3**–**8** and **10**

3		**4**		**5**		**6**		**7**		**8**		**10**	
(a) bond lengths		*(a) bond lengths*		*(a) bond lengths*		*(a) bond lengths*		*(a) bond lengths*		*(a) bond lengths*		*(a) bond lengths*	
Sb−Br1	2.7493(13)	Sb1−Br1	2.849(2)	Sb−Br1	2.5779(7)	Sb−Br1	2.6723(4)	Sb1−Br1	2.8023(18)	Sb1−Br1	2.5374(3)	Sb1−Br1	2.7463(4)
Sb−S1	2.780(2)	Sb1−Br3	2.8294(18)	Sb−Br2	2.9914(7)	Sb−Br2	2.8858(4)	Sb1−Br2	2.7144(17)	Sb1−Br2	2.6443(3)	Sb1−Br2	2.7637(5)
Sb−S2	2.782(2)	Sb1−Br2	3.233(2)	Sb−Br3	2.6457(7)	Sb−Br3	2.7608(3)	Sb1−Br3	3.0685(14)	Sb1−Br3	2.7347(3)	Sb1−Br3	2.5713(8)
S1−C1	1.707(7)	Sb1−S1	2.759(6)	Sb−S5	2.8085(14)	Sb−S1	2.8115(7)	Sb1−S12	2.577(4)	Sb1−S2	2.7936(8)	Sb1−Br3a	3.194(1)
S2−C8	1.715(7)	Sb1−S2	2.784(6)	Sb−S6	2.7002(14)	Sb−S2	2.5177(6)	Sb1−S22	2.514(3)	Sb1−S4	2.8427(7)	S−C1	1.655(4)
		S1−C1	1.705(19)	S5−C10	1.701(5)	S1−C1	1.739(3)	S12−C12	1.720(12)	S2−C1	1.691(3)		
		S2−C9	1.742(19)	S6−C1	1.714(5)	S2−C5	1.761(3)	S22−C22	1.742(12)	S4−C4	1.692(3)		
(b) angles		(b) angles		*(b) angles*		*(b) angles*		*(b) angles*		*(b) angles*		*(b) angles*	
Br1−Sb−S1	93.39(4)	Br1−Sb1−Br3	94.76(6)	Br1−Sb−Br2	87.63(2)	Br1−Sb−Br2	165.33(1)	Br1−Sb1−Br2	165.39(5)	Br1−Sb1−Br2	90.54(1)	Br1−Sb1−Br2	90.25(1)
Br1−Sb−S2	94.08(4)	Br2−Sb1−Br1	172.8(1)	Br1−Sb−Br3	92.02(2)	Br1−Sb−Br3	92.97(1)	Br1−Sb1−S12	79.54(10)	Br1−Sb1−Br3	87.82(1)	Br1−Sb1−Br3	88.12(3)
Br1−Sb−Br1a	180.00	Br2−Sb1−Br3	86.3(1)	Br1−Sb−S5	82.49(3)	Br1−Sb−S1	77.16(2)	Br1−Sb1−S22	76.42(8)	Br1−Sb1−S2	82.60(2)	Br1−Sb1−Br1a	180.00
Br1−Sb−S1a	86.61(4)	Br1−Sb1−S1	88.28(13)	Br1−Sb−S6	92.85(3)	Br1−Sb−S2	93.38(2)	Br2−Sb1−S12	90.67(10)	Br1−Sb1−S4	80.29(1)	Br1−Sb1−Br2a	89.75(1)
Br1−Sb−S2a	85.92(4)	Br1−Sb1−S2	91.34(13)	Br2−Sb−Br3	177.76(2)	Br2−Sb−Br3	97.50(1)	Br2−Sb1−S22	92.95(8)	Br2−Sb1−Br3	90.23(1)	Br1−Sb1−Br3a	91.88(3)
S1−Sb−S2	90.65(6)	Br3−Sb1−S1	98.56(11)	Br2−Sb−S5	94.43(3)	Br2−Sb−S1	91.97(2)	S12−Sb1−S22	90.22(10)	Br2−Sb1−S2	88.74(2)	Br2−Sb1−Br3	90.75(3)
Br1a−Sb−S1	86.61(4)	Br3−Sb1−S2	80.13(11)	Br2−Sb−S6	85.81(3)	Br2−Sb−S2	76.18(2)			Br2−Sb1−S4	169.99(2)	Br1a−Sb1−Br2	89.75(1)
S1−Sb−S1a	180.00	Br2−Sb1−S1	84.6(2)	Br3−Sb−S5	87.72(3)	Br3−Sb−S1	170.03(2)			Br3−Sb1−S2	170.35(2)	Br2−Sb1−Br2a	180.00
S1−Sb−S2a	89.35(6)	Br2−Sb1−S2	95.8(2)	Br3−Sb−S6	92.00(3)	Br3−Sb−S2	91.46(2)			Br3−Sb1−S4	93.40(2)	Br2−Sb1−Br3a	89.25(3)
Br1a−Sb−S2	85.92(4)	S1−Sb1−S2	178.61(15)	S5−Sb−S6	175.32(4)	S1−Sb−S2	87.76(2)			S2−Sb1−S4	86.13(2)	Br1a−Sb1−Br3	91.88(3)
S1a−Sb−S2	89.35(6)											Br2a−Sb1−Br3	89.25(3)
S2−Sb−S2a	180.00											Br3−Sb1−Br3a	180.00
Br1a−Sb−S1a	93.39(4)												
Br1a−Sb−S2a	94.08(4)												
S1a−Sb−S2a	90.65(6)												

3,4,5,6-tetrahydro-pyrimidine (0.116 g), 1.0 mmol of 2-mercaptopyridine (0.111 g), 1.0 mmol of 2-mercaptothiazoline (0.119 g), 1.0 mmol of 3-methyl-2-benzothiazolinthione (0.181 g), and 1.0 mmol of 2-mercaptopyrimidine (0.112 g) were dissolved in dichloromethane (10 cm^3) in the cases of preparation of **2**, **3**, **4**, **6**, **8** and in acetonitrile (10 cm^3) in the cases of preparation of **1**, **5**, **7**, **9**, **10**. A solution of antimony(III) bromide (0.181 g, 0.5 mmol) in methanol (10 cm^3) for **1**, **3**, **5**, **7**, **9**, **10** and in dichloromethane (10 cm^3) for **2**, **4**, **6**, **8** was then added to the above solution. The solution of **1**, **3**, **5**, **7**, **9**, and **10** were filtered off, and the resulting clear solutions were kept in darkness at room temperature to give crystals of the named **3**, **5**, **7**, **9**, and **10** except for **1**, which precipitated as a powder. In the cases of **2**, **4**, **6** and **8**, the solutions were stirred for 15 min and the resulting precipitations were filtered off and dried. Recrystallization of these solids from hot CH_3CN (20 cm^3) yielded crystals of **4**, **6**, and **8**, whereas **2** precipitated as a powder. All of the solid products are stable when kept in darkness at room temperature.

1: yellow powder; yield, 68%. Elemental analysis, Found: C, 4.39; H, 1.52; N, 10.62; S, 12.13. Anal. Calcd for $C_2H_8Br_3N_4S_2Sb$: C, 4.68; H, 1.57; N, 10.91; S, 12.48. IR (cm^{-1}): 3370m, 3282m, 3201m, 2361m, 1634s, 1405m, 1120w, 688m, 608m, 548m.

2: yellow powder; yield, 65%. Elemental analysis, Found: C, 16.69; H, 1.90; N, 9.88; S, 10.39. Anal. Calcd for $C_8H_{12}Br_3N_4S_2Sb$: C, 16.20; H, 2.05; N, 9.50; S, 10.87. IR (cm^{-1}): 3092s, 3000w, 2938w, 2884w, 1623w, 1570s, 1464s, 1350w, 1280m, 1154m, 1094m, 1017w, 917w, 738m, 669m, 511w.

3: orange crystals; yield, 40%. Elemental analysis, Found: C, 34.99; H, 2.37; N, 11.31; S, 12.80. Anal. Calcd for $C_{28}H_{26}Br_3N_8OS_4Sb$: C, 34.96; H, 3.03; N, 11.25; S, 12.87. IR (cm^{-1}): 3069m, 1617m, 1491s, 1450s, 1389w, 1365w, 1347s, 1254w, 1220w, 1165m, 1007m, 973m, 751s, 618w, 599s, 468w.

4: yellow crystals; yield, 65%. Elemental analyses, Found: C, 28.01; H, 2.11; N, 8.01; S, 9.55. Anal. Calcd for $C_{16}H_{16}Br_3N_4S_2Sb$: C, 27.85; H, 2.34; N, 8.12; S, 9.30. IR (cm^{-1}): 3129m, 1616m, 1448s, 1326m, 1184m, 803s, 719w, 626w, 538w.

5: brown crystals; yield, 65%. Elemental analyses, Found: C, 29.39; H, 2.56; N, 7.02; S, 8.32. Anal. Calcd for $C_{18}H_{22}Br_3N_4O_3S_2Sb$: C, 29.18; H, 3.09; N, 7.16; S, 8.20. IR (cm^{-1}): 3059s, 2973m, 1636s, 1500s, 1461s, 1384s, 1332m, 1258m, 1167s, 1117m, 1040m, 962w, 805m, 775w, 670w, 629w, 584m, 517w.

6: yellow crystals; yield, 69%. Elemental analyses, Found: C, 16.68; H, 2.82; N, 9.76; S, 10.99. Anal. Calcd for $C_8H_{16}Br_3N_4S_2Sb$: C, 16.18; H, 2.72; N, 9.43; S, 10.80. IR (cm^{-1}): 3328w, 3221m, 2971m, 1623s, 1590m, 1556s, 1438m, 1366m, 1317m, 1219m, 1072w, 812m, 688m, 623w, 560m, 412m.

7: orange crystals; yield, 54%. Elemental analyses, Found: C, 20.24; H, 1.69; N, 4.67; S, 10.63. Anal. Calcd for $C_{10}H_{10}Br_3N_2S_2Sb$: C, 20.57; H, 1.73; N, 4.80; S, 10.99. IR (cm^{-1}): 3429m, 2910w, 1582s, 1511m, 1439w, 1368w, 1261m, 1127m, 761s, 485m.

8: yellow crystals; yield, 75%. Elemental analyses, Found: C, 12.22; H, 1.46; N, 4.23; S, 21.02. Anal. Calcd for $C_6H_{10}Br_3N_2S_4Sb$: C, 12.01; H, 1.68; N, 4.67; S, 21.38. IR (cm^{-1}): 3449w, 3263s, 2362m, 1514s, 1339w, 1302m, 1042m, 991w, 926w, 614w, 425w.

9: yellow crystals; yield, 54%. Elemental analyses, Found: C, 26.27; H, 1.91; N, 10.61; S, 12.12. Anal. Calcd for $C_{16}H_{14}Br_3N_2S_4Sb$: C, 26.54; H, 1.95; N, 10.91; S, 12.48. IR (cm^{-1}): 3446m, 2361m, 1459s, 1426m, 1348s, 1313m, 1262m, 1141m, 1096s, 967s, 752s, 638w, 522m, 423w.

10: orange crystals; yield, 30%. Elemental analyses, Found: C, 12.68; H, 1.38; N, 7.55; S, 9.07. Anal. Calcd for $C_8H_{10}Br_5N_4S_2Sb$:

Table 2. Gas and Dichloromethane Phase B3LYP/6-31G(d) Calculated Energy, Charge for S Atoms, HOMO, LUMO and Nucleophilicity (n), Values of Ligands

	Gas Phase					Dichloromethane Phase				
ligands	energy (Hartrees)	charge(S) (e)	HOMO (Hartrees)	LUMO (Hartrees)	nucleophlicity[a] (Hartrees)	energy (Hartrees)	charge(S) (e)	HOMO (Hartrees)	LUMO (Hartrees)	nucleophlicity[a] (Hartrees)
TU	−548.2156	−0.30	−0.4079	−0.0069	−0.4011	−548.2299	−0.41	−0.4064	0.0124	−0.4189
MMI	−664.9445	−0.32	−0.2002	0.0036	−0.2038	−664.9597	−0.40	−0.2055	0.0051	−0.2106
MBZIM	−778.0771	−0.30	−0.3457	−0.0305	−0.3152	−778.0907	−0.37	−0.3421	−0.0272	−0.3150
MMBZIM	−817.3947	−0.30	−0.1980	−0.0297	−0.1683	−817.4082	−0.37	−0.1994	−0.0269	−0.1725
EtMBZIM	−931.9172	−0.31	−0.1911	−0.0254	−0.1657	−931.9363	−0.38	−0.1928	−0.0234	−0.1694
tHPMD	−664.9506	−0.36	−0.3536	0.0107	−0.3644	−664.9684	−0.45	−0.3448	0.0107	−0.3556
PYT	−646.4803	−0.31	−0.2011	−0.0578	−0.1433	−646.4914	−0.38	−0.2028	−0.0559	−0.1470
MTZD	−968.4629	−0.23	−0.2135	−0.0328	−0.1807	−968.4777	−0.31	−0.2162	−0.0309	−0.1853
MMBZT	−1160.2149	−0.22	−0.2109	−0.0456	−0.1652	−1160.2246	−0.28	−0.2136	−0.0471	−0.1665
PMT	−662.5103	−0.25	−0.2076	−0.0751	−0.1325	−662.5252	−0.34	−0.2126	−0.0726	−0.1400

[a] $n = E_{HOMO} - E_{LUMO}$.

Table 3. Cytostatic Activity of the Compounds Against murine Leukemia Cells (L1210), Murine Mammary Carcinoma Cells (FM3A), Human T-Lymphocyte (Molt4/C8, CEM) and Human Cervix Carcinoma (HeLa) Cells

	IC_{50}[c] (μg/ml)					MCC[b] (μg/ml)		
Sb(III) bromide compound	L1210	FM3A	Molt4/C8	CEM	Hela	Hel	Hel	ref
$[SbBr_3(TU)_2]$ (**1**)	20 ± 9	47 ± 1	12 ± 2	55 ± 21	12 ± 0	5.6 ± 3.5	100	[c]
$[SbBr_3(MMI)_2]$ (**2**)	42 ± 14	72 ± 1	27 ± 12	75 ± 25	17 ± 2	22 ± 17	500	[c]
$\{[SbBr_2(MBZIM)_4]^+ [Br]^- H_2O\}$ (**3**)	42 ± 15	66 ± 1	21 ± 9	67 ± 11	20 ± 2	12 ± 1	500	[c]
$\{[SbBr_2(\mu_2\text{-}Br)(MMBZIM)_2]_2\}$ (**4**)	24 ± 6	52 ± 8	14 ± 2	50 ± 7	14 ± 2	15 ± 1	500	[c]
$\{[SbBr_2(\mu_2\text{-}Br)(EtMBZIM)_2]_2$ MeOH$\}$ (**5**)	41 ± 11	64 ± 2	26 ± 3	42 ± 2	16 ± 0	<8	≥100	[c]
$\{[SbBr_3(\mu_2\text{-}S\text{-}tHPMT)(tHPMT)]_n\}$ (**6**)	22 ± 6	54 ± 4	16 ± 6	63 ± 20	14 ± 1	12 ± 0	500	[c]
$\{[SbBr_2(\mu_2\text{-}Br)(PYT)_2)_n\}$ (**7**)	19 ± 3	56 ± 6	13 ± 3	42 ± 16	3.7 ± 0.5	9.3 ± 0.0	≥20	[c]
$\{[SbBr_2(\mu_2\text{-}Br)(MTZD)_2]_n\}$ (**8**)	23 ± 8	53 ± 1	15 ± 4	59 ± 11	15 ± 0	12 ± 2	500	[c]
$[SbBr_3(MMBZT)_2]$ (**9**)	43 ± 28	57 ± 8	15 ± 6	31 ± 17	16 ± 2	17 ± 12	500	[c]
$\{[SbBr_5]^{2-}[(PMTH_2^+)_2]\}$ (**10**)	15 ± 3	37 ± 4	9.4 ± 0.8	44 ± 25	3.1 ± 1.2	5.9 ± 1.2	20	[c]
$\{[SbCl_2(MBZIM)_4]^+ \cdot Cl^- \cdot 2H_2O \cdot (CH_3OH)\}$	10.8	32.3	21.5	80.7	5.7			[11]
$\{[SbCl_2(MBZIM)_4]^+ \cdot Cl^- \cdot 3H_2O \cdot (CH_3CN)\}$	17.3	76.1	25.9	76.1	6.1			[11]
$[SbCl_3(MBZIM)_2]$	16.4	54.4	23.8	59.2	4.1			[11]
$[SbCl_3(EtMBZIM)_2]$	12.9	25.3	9.2	14.8	4.3			[11]
$[SbCl_3(MTZD)_2]$	13.5	26.1	14.9	57.8	3.2			[11]
$[SbCl_3(tHPMT)_2]$	13.4	42.4	17.5	54.3	3.5			[11]
cisplatin	0.07		0.1		3.0			20a, b
carboplatin					<11			20a[a]

[a] 50% inhibitory concentration or compound concentration required to inhibit tumor cell proliferation by 50%. [b] Minimal cytotoxic concentration required to cause a microscopically visible alteration of cell morphology. [c] This work.

Table 4. Structure Refinement Details for **3**−**8** and **10**

	3	**4**	**5**	**6**	**7**	**8**	**10**
empirical formula	$C_{28}H_{26}Br_3N_8OS_4Sb$	$C_{16}H_{16}Br_3N_4S_2Sb$	$C_{19}H_{24}Br_3N_4O_3S_2Sb$	$C_8H_{16}Br_3N_4S_2Sb$	$C_{10}H_{10}Br_3N_2S_2Sb$	$C_6H_{10}Br_3N_2S_4Sb$	$C_8H_{10}Br_5N_4S_2Sb$
fw	996.34	689.93	782.02	593,84	583.80	599.89	Monoclinic
T (K)	100(2)	100(2)	100(2)	100(2)	293	100(2)	100(2)
cryst syst	Monoclinic	Triclinic	Triclinic	Monoclinic	Orthorhombic	Monoclinic	Monoclinic
space group	$P2_1/c$	$P\bar{1}$	$P\bar{1}$	$P2_1/c$	$Ccca$	$P2_1/c$	$P2_1/n$
a (Å)	13.806(5)	8.8226(13)	9.0708(2)	9.7370(6)	10.831(2)	8.5545(3)	5.7512(1)
b (Å)	16.935(7)	11.2837(17)	9.2943(2)	20.7721(10)	28.157(6)	14.8824(4)	15.1339(4)
c (Å)	7.808(3)	12.505(2)	15.3618(4)	8.7033(4)	25.489(5)	12.2796(3)	10.5575(3)
α (deg)	90	110.002(14)	78.752(2)	90	90	90	90
β (deg)	98.262(5)	91.959(13)	87.505(2)	107.507(5)	90	100.417(3)	104.248(3)
γ (deg)	90	102.982(13)	86.356(2)	90	90	90	90
V (Å^3)	1806.6(12)	1131.5(3)	1267.02(5)	1678.77(16)	7773(3)	1537.57(8)	890.64(4)
Z	1	2	2	4	8	4	2
ρ_{calcd} (g/cm^3)	1.864	2.013	1.986	2.350	2.125	2.592	2.788
μ (mm^{-1})	4.4	6.7	6.0	9.0	8.8	10.1	13
R, wR, S	0.044, 0.077, 0.72	0.069, 0.203, 1.00	0.033, 0.071, 0.93	0.019, 0.041, 0.96	0.067, 0.207, 1.05	0.019, 0.038, 0.92	0.022, 0.051, 0.97

C, 12.85; H, 1.35; N, 7.49; S, 8.58. IR (cm^{-1}): 3443m, 2895m, 2361m, 1600s, 1547m, 1377w, 1263m, 1190s, 988m, 773m, 625w, 465m.

X-ray Structure Determination. Intensity data for the colorless crystals of **3**, **4**, **5**, **6**, **8**, and **10** were collected on an Oxford Diffraction CCD instrument,[22a] using graphite-monochromated Mo radiation ($\lambda = 0.71073$ Å), whereas a KUMA KM4CCD four-circle diffractometer[22b] with a CCD detector used for **7**, using graphite-monochromated Mo radiation ($\lambda = 0.71073$ Å). Cell parameters were determined using up to 9402 reflections.[22c]

All data were corrected for Lorentz-polarization effects and absorption.[22a,c] The structures were solved with direct methods with *SHELXS97*[22d] and refined by full-matrix least-squares procedures on F^2 with *SHELXL97*.[22e] All non-hydrogen atoms were refined anisotropically, and hydrogen atoms were located at calculated positions and refined via the "riding model" with isotropic thermal parameters fixed at 1.2 (1.3 for CH_3 groups) times the U_{eq} value of the appropriate carrier atom. Significant crystal data are given in Table 4.

The crystal structure of **3** could be refined better (with regard to both the R factors and displacement parameters) if the

counteranion is defined as a disorder Br^-/OH^- (53/47). This may have occurred because of a hydrolysis process that took place during the preparation. The strange shape of Br3 ellipsoid in the case of the structure of **7** is probably the result of a disorder.

Supplementary data are available from the CCDC, 12 Union Road, Cambridge CB2 1EZ, U.K., (e-mail: deposit@ccdc.cam.ac.uk), on request, quoting the deposition nos. CCDC-702615 (**3**), 702617 (**4**), 702615 (**5**), 702620 (**6**), 702619 (**8**) and 702618 (**10**), respectively, and CCDC-704581 for **7**.

X-ray Powder Diffraction. X-ray powder diffraction patterns, from powders derived from the crushed, were obtained using a Bruker AXS D8 Avance diffractometer in Bragg−Brentano geometry equipped with a Cu sealed-tube radiation source (λ = 1.54178 Å) and a secondary beam graphite monochromator. The 2θ range used in the measurements was from 5° to 50° in steps of 0.02° with a count time of 10 s per step.

Computational Studies. All of energies were calculated with DFT Becke3-LYP method[23a−d] together with the standard basis sets 6-31G(d)[23e,f] as implemented in the *Gaussian 98* program.[23g] The total energies are given in Hartrees using the conversation factor 1 Hartree = 627.5095 kcal mol^{-1}.

Cytostatic Activity Assays. Murine leukemia L1210, murine mammary carcinoma FM3A, human T-lymphocyte Molt 4 and CEM, and human cervix carcinoma HeLa cells were suspended at 300 000−500 000 cells/ml in RPMI-1640 culture medium supplemented with 10% fetal bovine serum and 2 mM L-glutamine, and 100 μL of a the cell suspensions were added to 100 μL of an appropriate dilution of the test compounds in 96 well microtiter plates. After incubation at 37 °C for two (L1210 and FM3A) or three (Molt4, CEM and HeLa) days, the cell number was determined using a Coulter counter. The number of the suspension cells could be counted directly; the number of the monolayer HeLa cells were counted after detachment of the cells upon trypsinization. The IC_{50} was defined as the compound concentration required to inhibit cell proliferation by 50%.

Acknowledgment. This research was carried out in partial fulfillment of the requirements for the Ph.D. thesis of I.I.O. within the graduate program in Bioinorganic Chemistry at the University of Ioannina. S.K.H., N.H., H.S, and I.S.B. would like to acknowledge a NATO grant for the exchange of scientists. I.I.O. would like to thank the Hellenic Ministry of Education for a scholarship for postgraduate studies. The research of J.B. was supported by grant GOA no. 05/19.

Note Added after ASAP Publication. This article was published ASAP on January 26, 2009, with minor text errors in equations II and III. The corrected article was published ASAP on February 2, 2009.

IC8019205